1 **Impact of Lagrangian Sea Surface Temperature Variability on Southern**
2 **Ocean Phytoplankton Community Growth Rates**

3

4 **Jessica Zaiss[1], Philip W. Boyd[2], Scott C. Doney[3], Jon N. Havenhand[4], Naomi M. Levine[5]**

5

6 [1]Department of Earth Science, University of Southern California

7 [2]Institute for Marine and Antarctic Studies, University of Tasmania

8 [3]Department of Environmental Sciences, University of Virginia

9 [4]Department of Marine Science, University of Gothenburg

10 [5]Department of Marine and Environmental Biology, University of Southern California

11 Corresponding author: Jessica Zaiss (zaissbow@usc.edu)

12

13

14 **Key Points:**

15 • Sea surface temperature (SST) variability differs between the Lagrangian and Eulerian
16   reference frames

17 • SST variability decreases phytoplankton community growth rates for multiple
18   generations

19 • The Q_{10} growth model does not fully capture the effects of sea surface temperature
20   variability on phytoplankton growth

21

22

23

24

25

26

27

28

29

Abstract

30

31 Ocean phytoplankton play a critical role in the global carbon cycle, contributing ~50% of global
32 photosynthesis. As planktonic organisms, phytoplankton encounter significant environmental
33 variability as they are advected horizontally across the upper ocean. The impact of this
34 variability on phytoplankton growth rates has not been quantified and is not captured by many
35 current biogeochemical models. Here, we systematically investigated the impact of different
36 rates and magnitudes of sea surface temperature (SST) variability on phytoplankton community
37 growth rates using surface drifter observations from the Southern Ocean ($> 30^{\circ}$S) and a
38 phenotype-based ecosystem model. Moderate SST changes of 3-5°C over 7-21 days (~4-13
39 generations for a typical growth rate of 0.5 day^{-1}) produced the largest time lag between the
40 temperature change and the biological response. Shorter term SST variability (<7 days) had little
41 impact on the phytoplankton community growth rates. The impact of SST variability was not
42 captured by the Q_{10}-based model of community growth leading to an overestimation of
43 community growth rates, particularly in dynamic, strong frontal regions of the Southern Ocean.
44 Furthermore, we demonstrated that the nature of variability encountered in a Lagrangian
45 reference frame (following trajectories of surface water parcels) differed from that within an
46 Eulerian reference frame, which resulted in significant effects on phytoplankton dynamics. Our
47 results quantify the temporal scales of SST variability relevant for phytoplankton in the Southern
48 Ocean and take a first step towards including the impact of variability and biological response
49 times into numerical models.

50

Plain Language Summary

51

52 Ocean phytoplankton are fundamental to the global carbon cycle. To understand the sensitivity
53 of the global carbon cycle to shifts in climate, we need to understand the impact of
54 environmental variability on phytoplankton growth rates. Phytoplankton encounter
55 environmental variability (e.g. sea surface temperature (SST) changes) in a Lagrangian reference
56 frame. Here, we quantified the variability in SST encountered by phytoplankton *in situ* using
57 surface drifters and investigated the impact of this variability on phytoplankton community
58 growth rates using a phenotype-based ecosystem model. We also compared SST variability in
59 the Lagrangian reference frame to the Eulerian reference frame using high-resolution satellite
60 data. We found significant differences between the two reference frames with larger SST
61 changes in the Lagrangian than in the Eulerian reference frame, and that these differences
62 impacted phytoplankton community structure and growth rates. SST changes >0.07 $^{\circ}$C/day
63 induced a lag time between SST changes and the biological response. The impact of SST
64 variability was not captured by the Q_{10} model that is typically used by global biogeochemical
65 models. Our results quantify the temporal scales of SST variability relevant for Southern Ocean
66 phytoplankton and provide a first step towards implementing the biological response to
67 variability into numerical models.

68

69   **1. Introduction**

70   The ocean is a highly dynamic environment and, in some regions, is expected to become more
71   variable with rising global temperatures (Boyd et al., 2016). Previous work investigating the
72   impact of anthropogenic warming on marine planktonic ecosystems has primarily focused on
73   shifts in the annual mean and/or seasonal conditions. However, recent work has highlighted the
74   importance of considering changes in sub-annual temperature variability, in addition to changes
75   in the mean state (Doblin & van Sebille, 2016; Kroeker et al., 2020). Such short-term variability
76   may be particularly important for phytoplankton dynamics as both mean environmental
77   conditions and sub-seasonal variability affect plankton physiology (Kremer et al. 2018). To
78   better understand how phytoplankton might respond to future environmental changes, such as
79   warming, it is important to characterize the variability these phytoplankton encounter *in situ* and
80   determine the influence of that variability on physiology and community structure.

81

82   Phytoplankton are largely passive drifters and, so a Lagrangian, rather than Eulerian, reference
83   frame is most appropriate when considering environmental variability. Both mean conditions and
84   variability (magnitude and rate of change) can differ markedly between the two reference frames
85   (e.g. Doblin and van Sebille 2016; Hellweger et al. 2016). As a result, the temperature regime
86   that sets the thermal acclimation history of a phytoplankton community may differ from
87   prevalent local conditions. For example, Hellweger et al. (2016) modeled the advection of
88   communities across large temperature gradients, such as those along a western boundary current,
89   and showed that the optimum growth temperature (T_{opt}) for the community can be considerably
90   different from the *in situ* temperature. However, the impact on the community growth rate and
91   the extent of differences in the characteristics of Lagrangian versus Eulerian variability – and the
92   circumstances under which these differences have the largest impact on phytoplankton
93   community dynamics – remain unclear.

94

95   In global marine ecosystem models, temperature-dependent phytoplankton growth rates are often
96   parameterized via a Q_{10} model based on thermal performance curves generated across multiple
97   temperatures under constant conditions. The Q_{10} parameterization assumes rapid phenotypic
98   shifts by the community such that, as the temperature changes, the community rapidly shifts its
99   optimal growth temperature (Eppley, 1972). Previous modeling studies have demonstrated that
100   the Q_{10} growth parameterization does not capture phytoplankton population dynamics, such as
101   the time-lag between changes in sea surface temperature (SST) and the corresponding change in
102   optimum growth temperature of the community (Hellweger et al. 2016), and results in an over-
103   estimation of phytoplankton community growth rates (Moisan et al., 2002). Additionally, in a lab
104   culture study, Bernhardt et al., (2018) demonstrated that due to non-linearities, fluctuating
105   conditions will alter the shape of the thermal performance curve relative to a constant
106   environment. An improved understanding of temperature-dependent growth rates and how to
107   parameterize these relationships in global models is critical as they have been shown to be one of

108   the main sources of uncertainty for future climate predictions among global biogeochemical
109   models (Laufkötter et al., 2015).

110

111   It has been suggested that phytoplankton responses to changes in temperature depend on
112   previous thermal history (previous acclimation temperature), as well as the magnitude of change
113   and rate of change (Kremer et al., 2018; Pittera et al., 2014). However, results from lab-based
114   studies remain inconclusive. Some studies found an overall decrease in community growth rate
115   in a thermally variable environment relative to a stable environment (Bernhardt et al., 2018; Qu
116   et al., 2019; Wang et al., 2019), while others found higher growth rates under variable conditions
117   (Schaum et al., 2018), and some found that thermal variability did not impact community
118   growth rates (Kling et al., 2019; Qu et al., 2019). The lack of consensus concerning the impact of
119   variability on phytoplankton growth rates may be due to the different magnitudes and rates of
120   change used by the different studies, which ranged from ~1.5°C/day (Schaum et al., 2018) to as
121   high as 10°C/day (Bernhardt et al., 2018).

122

123   The direction of SST change, either increasing or decreasing, can also impact the community
124   growth rate due to asymmetry in the thermal reaction norm (Moisan et al., 2002). For
125   phytoplankton in the Southern Ocean, the shape of the reaction norm can be broad and
126   symmetrical, but for most species tends to be asymmetric, often with skewed tails towards lower
127   temperatures (Boyd, 2019). The growth response to changes in SST will depend on the starting
128   SST relative to the optimum growth temperature (T_{opt}) and whether the SST change is increasing
129   or decreasing (Figure 1). When the starting temperature is along the skewed tail and there is an
130   increase in SST, the growth rate will increase (orange arrow, Figure 1). If the starting SST is near
131   T_{opt}, an increase in SST will move beyond the optimum growth and growth rates will decrease
132   (red arrow, Figure 1). Phytoplankton with skewed reaction norms living in water with
133   temperatures at or near T_{opt} can persist through larger decreases in SST than they can increases in
134   SST. Depending on the starting SST, the change in growth rate associated with changing SSTs
135   can either be linear or exponential and the rate of change in growth rate will depend on the
136   acclimation rate and type of acclimation or plasticity (i.e. detrimental or beneficial; Kremer et al.,
137   2018) of the phytoplankton. A detrimental response is one in which the initial growth rate after
138   the temperature shift is greater than the acclimated rate and acclimation to the new temperature
139   results in a decrease in growth rate. A beneficial response is one in which growth rates fall below
140   the acclimated growth rate immediately after the temperature shift but then increase to the
141   acclimated growth rate. When SST changes are slower than the phytoplankton acclimation rate,
142   the instantaneous growth rate will be equivalent to the acclimated growth rate. When the rate of
143   SST change is faster than the rate of acclimation, the instantaneous growth rates could be higher
144   or lower than the acclimated growth rate, depending on the type of response, detrimental or
145   beneficial, respectively (Kremer et al., 2018).
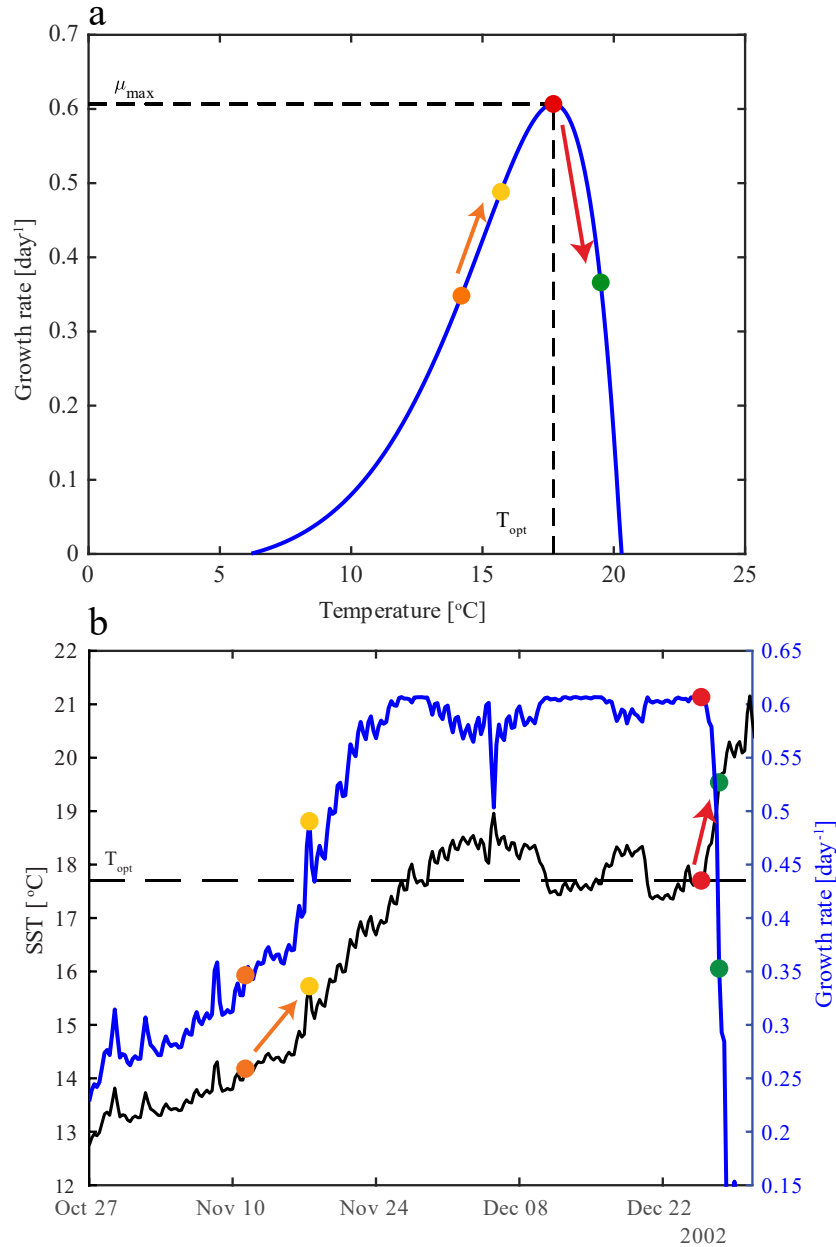
146

Figure 1. The impact of SST variability on individual phenotype growth rate. (a) The temperature related growth response for a phenotype with a skewed shaped reaction norm. The values for the optimum growth temperature (T_{opt}) and the corresponding maximum growth rate (μ_{max}) are shown with dashed lines. (b) The 90-day SST profile of an example drifter trajectory (black) and the associated changes in phenotype growth rate (blue). The orange and red arrows in the top panel indicate the change in phenotype growth rate associated with the corresponding changes in SST in the bottom panel.

156   Here, we provide a systematic assessment of the effect of different magnitudes and rates of
157   change of temperature on community growth rates and how those might relate to the variability
158   encountered by phytoplankton communities *in situ*. Specifically, using *in situ* and remote sensing
159   SST observations from the Southern Ocean (south of 30°S), we constrained the relevant
160   frequencies and magnitudes of temperature variability that phytoplankton encounter in the
161   Lagrangian reference frame. This southern hemisphere region encompasses some of the lowest
162   (0.2°C) and highest (1.5°C), non-seasonal SST variability globally (Deser et al., 2010) which
163   provided a large range over which to investigate the impact of temperature variability on
164   phytoplankton community growth rates. We used a suite of idealized simulations of temperature
165   shifts and a numerical model to provide mechanistic insight into how this variability might
166   impact community growth rates. We found that relatively small perturbations (< 2 °C over 7
167   days), which are most common *in situ*, did not substantially impact community growth rates and
168   that moderate changes (4-6°C over 21-45 days) had the largest and longest lasting effect on
169   community growth rates. These moderate changes resulted in a temporary decrease in
170   community growth rate that lasted up to 20 generations, as the community responded to the new
171   temperature. Applying our numerical model to *in situ* SST data from the Southern Ocean, we
172   found that the effect of temperature variability on phytoplankton community growth rates was
173   present everywhere in Southern Ocean with the largest impact occurring in regions dominated by
174   meso- and sub-mesoscale activity.

175

176   **2. Methods**

177   The impact of SST variability on phytoplankton community growth rates was studied by
178   combining SST observations, both *in situ* and from remote sensing products, and a phenotype-
179   based ecosystem model. Here, we focused on the impact of SST variability on phytoplankton
180   community growth rates and therefore did not consider growth limitations due to other sources of
181   variability such as nutrients, light, and mixed layer depth (Rohr et al., 2020a, 2020b). Further
182   work is needed to investigate these multi-driver impacts.

183

184   *2.1 Southern Ocean drifter profiles*

185   Lagrangian SST data were obtained from 422 Southern Ocean surface drifters from the Global
186   Drifter Program with 6-hourly SST data. Float data south of 30°S from July 1999 – April 2016
187   was downloaded from the Drifter Data Centre at the Atlantic Oceanographic and Meteorological
188   Laboratory (accessed 11/2018). The lifetime of the drifters ranged from 91 days to 5.8 years
189   with a median duration of 521 days. Each drifter was segmented into 90-day trajectories to
190   provide consistency in the dataset. We used only segments that had less than 10% of missing
191   data. This resulted in 2,190 90-day trajectories (Figure 2a).

192

193   The surface drifter trajectories were used to examine SST variability within a Lagrangian
194   reference frame over different temporal periods. Seasonal dynamics dominated the longer time
195   frames (90 days) while smaller-scale dynamics were important for the shorter windows. We
196   chose to include seasonal dynamics in the analysis rather than filter them out as they were
197   important sources of SST variability encountered by phytoplankton. While surface drifters may
198   have been subjected to some physical movements that phytoplankton do not encounter (e.g.,
199   lateral transfer across fronts due to wind rather than subduction and mixing), they provided the
200   best *in situ* dataset for studying Lagrangian variability in surface temperature. To minimize this
201   impact, we limited our analysis to the most frequently measured scales of variability within the
202   drifter record (Section 3.1).

203

204   To estimate the magnitude of Lagrangian variability in our study region, we applied moving
205   windows of 7, 21, 45, and 90 days to each of the 90-day trajectories and recorded the absolute
206   value of the maximum range of SST recorded by the drifter during each window (ΔSST_{max}) and
207   the time (Δt_{max}) over which the temperature change occurred. To assess the distribution of
208   variability across different window sizes, we aggregated the data into 1°C bins for ΔSST_{max} and
209   Δt_{max} bins of 0-7, 8-21, 22-45, and 46-90 days. For example, a 2.4^{o}C change that occurred over
210   14 days was recorded in the 2-3°C and 8-21-day bin. To investigate the potential impact of
211   small-scale noise, we also created smoothed splines of each of the 90-day SST profiles using a
212   cubic smoothing spline (*csaps* in Matlab with a smoothing parameter of 0.00001). We then
213   repeated the ΔSST_{max} and Δt_{max} analysis on the spline data.

214

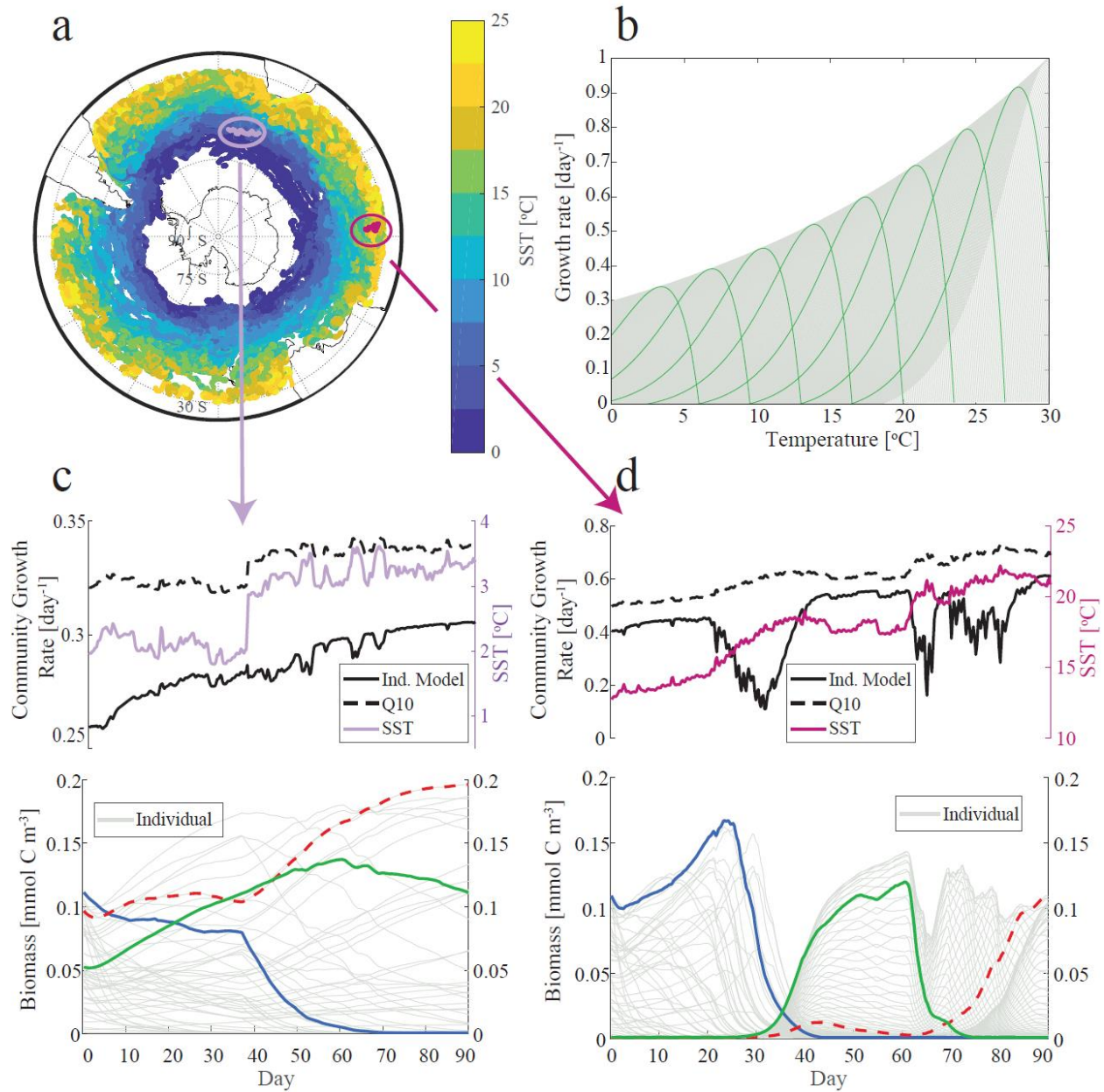Figure 2. a) Map of all 90-day drifter trajectories (n = 2190) colored by SST. Two example trajectories are highlighted in purple and magenta. b) Reaction norms for each of the 319 phenotypes in the ecosystem model. The grey lines represent all the phenotype reaction norms and the green lines are example phenotypes to highlight the reaction norm shape. c and d) Example trajectories and their resulting model outputs. The top panels show the SST (colors), the community growth rate simulated by Q_{10} method (dashed line), and the community growth rate from our phenotype-based model (solid line). The bottom panel shows the growth rate through time of each phenotype (grey lines). The blue line follows the phenotype with the highest initial biomass, the red dashed line follows the phenotype that has the highest biomass at the end of the 90 days, and the green line follows the phenotype that has a T_{opt} equal to the mean SST of the trajectory.

227   *2.2 Remote sensing SST*

228   To compare the SST variability in the Lagrangian reference frame to the variability that would
229   be captured in the Eulerian reference frame, we used high-resolution (0.01° horizontal resolution
230   and 1 day temporal resolution) satellite SST data from GHRSST Level 4 MUR Global
231   Foundation Sea Surface Temperature Analysis (v4.1) (JPL MUR MEaSUREs Project, 2015;
232   accessed Oct. 2018). This dataset spanned 2003-2014 which overlaps with 71% of our 90-day
233   drifter trajectories. For each 90-day drifter segment between 2003-2014, we extracted 90 days of
234   satellite SST data for the latitude and longitude of the final location of the drifter, where the 90
235   days corresponded to the dates of the drifter segment. We performed the same ΔSST_{max} and Δt_{max}
236   variability analyses for the satellite data as the surface drifter trajectories (described in Section
237   2.1).

238

239   *2.3 Idealized SST profiles*

240   We complemented the observed SST trajectories with idealized SST trajectories to
241   mechanistically understand the impact of the rate and magnitude of SST change on community
242   growth rates. Specifically, a suite of trajectories (N = 64) was generated with both increasing and
243   decreasing SST trends ranging from $\Delta SST = 2°$ to $\Delta SST = 9°C$ (in increments of 1°C) over 7, 21,
244   45, and 90 days. This range was chosen based on our Lagrangian variability analysis. To
245   minimize initialization bias, SST was held constant for the first 30 days before
246   increasing/decreasing. After the SST change, the SST was again held constant until the 200th
247   day. The final temperature for all idealized trajectories was 15°C. The impact of the final
248   temperature on model results was analyzed with a set of sensitivity experiments. The final SST
249   had no significant impact on the results when the results were reported in terms of generation,
250   rather than absolute days as this normalized the effect of higher growth rates at warmer
251   temperatures (Supplemental Information S1).

252

253   *2.4 Phenotype-based Ecosystem Model*

254   To estimate the impact of variable temperature on phytoplankton community growth rates, we
255   used a phenotype-based ecosystem model. The model consisted of 319 phytoplankton
256   phenotypes that were identical except for the optimum growth temperatures (T_{opt}). Temperature
257   dependent growth rate (μ, day^{-1}) was defined as a function of T (°C) (Thomas et al., 2012):

$$\mu(T) = ae^{bT}\left[1 - \left(\frac{T-T_{opt}}{w/2}\right)^2\right]$$ Eq. 1

259

260   where T_{opt} was the optimal growth temperature. The value of b controlled the shape of the
261   reaction norm, a (day^{-1}) scaled the reaction norm, and w (°C) defined the width of the reaction
262   norm. We used two sets of reaction norms: a symmetrical, or broad, curve where $b = 0$ (°C^{-1}) and

263 a skewed reaction norm where b = 0.3 ($^{\circ}$C^{-1}). Both curves had a thermal breadth of 14°C (w = 20
264 $^{\circ}$C), consistent with observed reaction norms for many polar species (Boyd, 2019). Sensitivity
265 tests were performed with thermal breadths of 10.5°C (w = 15 $^{\circ}$C) and 20.5°C (w = 29 $^{\circ}$C)
266 (Supplemental Information). The results from these sensitivity tests did not differ substantially
267 from the simulations with a thermal breadth of 14°C.

268

269 The parameter *a* scaled the reaction norms at T_{opt} to the Eppley curve (Eppley, 1972) where
270 maximum growth rates ranged between 0.28 - 1.0 day^{-1} for -1.8°C to 30°C, consistent with
271 experimental data (Boyd, 2019). Specifically, a_i was defined for each phenotype *i* as:

$$a_i = 0.2963e^{0.0405T_{opt}} \qquad \text{Eq. 2}$$

273 This resulted in a Q_{10} relationship of 1.5, consistent with the apparent Q_{10} from Sherman et al.
274 (2016). We generated 319 phenotype curves for both the broad and skewed reaction norms with
275 T_{opt} ranging from   -1.8 $^{\circ}$C to 30 $^{\circ}$C increasing by 0.1 $^{\circ}$C (Figure 2a).

276

277 The biomass of each phytoplankton phenotype P_i was calculated at each time-step as the integral
278 of:

$$\frac{dP_i}{dt} = \mu_i(T)P_i - m(T)P_i^2 \qquad \text{Eq. 3}$$

280 where $\mu_i(T)$ was the temperature-dependent growth rate for phenotype *i* from Equation 1. $m(T)$
281 was the temperature-dependent quadratic mortality rate (m^3 mmol C^{-1} day $^{-1}$) where:

$$m(T) = 0.1*a \qquad \text{Eq. 4}$$

283 Here we used the same temperature dependent Eppley curve (Eq. 2) to scale mortality with
284 temperature using SST instead of T_{opt} where *a* = 1 day^{-1} for SST = 30°C . We imposed a
285 minimum biomass (0.001 mmol C m^{-3}) so that no phenotype went locally extinct, akin to the
286 "everything is everywhere" principle (Hutchinson, 1961). Sensitivity tests were performed with
287 the minimum biomass set to 0.0001 mmol C   m^{-3}. The minimum biomass threshold did not
288 affect the overall patterns but did increase both the magnitude of the difference from the
289 community growth rates obtained using the Q_{10} model and the time to acclimation (memory
290 length, Section 3.2) for both broad and skewed reaction norms (Supplemental Information).
291 Imposing this minimum biomass purposefully introduced mass into the system which was
292 accounted for by adjusting the biomass of each phenotype to keep the total community biomass
293 at the concentration it would have been without the minimum biomass criteria. Specifically, the
294 total change in biomass without the minimum biomass phenotypes was calculated using the
295 biomass weighted community growth rate (λ) in place of $\mu(T)$ in Eq. 3, where λ was defined as:

$$\lambda = \sum \mu_{i,t} \frac{P_{i,t}}{P} \qquad \text{Eq. 5}$$

297   where, $\mu_{i,t}$ was the growth rate of the *ith* phenotype at time *t* for all phenotypes with biomass

298   greater than the minimum, $P_{i,t}$ was the biomass of the *ith* phenotype whose biomass was greater

299   than the minimum at time *t*, *P* was the sum of the biomass of all phenotypes with biomass greater

300   than the minimum at time *t*.

301

302   Several different models for mortality and grazing were tested including linear mortality,

303   constant mortality, a dynamic zooplankton population, and a simple ecosystem model with

304   constant grazing pressure (see section S.4 in Supplemental Material). All model versions resulted

305   in qualitatively similar results which demonstrated that the community dynamics were not

306   particularly sensitive to the top-down control formulation in the model (Section S.4 in

307   Supplemental Material). Here, we present the quadratic mortality as it was the simplest model

308   with smooth (non-oscillatory) solutions.

309

310   The ecosystem model was forced with each of the 2,190 drifter segment trajectories (see Figure

311   2c-e for examples), the corresponding smoothed splines, the idealized SST profiles, and the

312   satellite-derived SSTs. The initial biomass of phenotypes with a T_{opt} within ± 2.5°C of the

313   starting SST value were randomized to simulate previously accumulated biomass with

314   phenotypes outside this range set to the minimum biomass. Simulations that used idealized SST

315   profiles were performed 100 times with different initial biomass conditions to account for

316   stochasticity in the model initialization.

317

318   3. Results

319   *3.1 SST variability*

320   We characterized *in situ* SST variability using the surface drifter SST data. The average ΔSST_{max}

321   values ranged from 0.9°C ± 0.7°C (1σ) for the 7-day window, which corresponded to 0.13°C/day

322   change over the 7 days, to 4.2°C ± 2.0 °C (1σ) for the 90-day window or 0.05°C/day change

323   (Figure S8, Table S1). The latter was consistent with the expected seasonal SST cycle for the

324   Southern Ocean (Reynolds & Smith, 1994). The SST variability of the drifters was highly

325   correlated with ΔSST_{max} (Figure S9).

326

327   Using the ΔSST_{max} analysis, we were able to quantify the most common types of variability

328   encountered *in situ* in terms of both the magnitude of change and the rate of change (Figure 3a).

329   Due to the difference in the number of data points generated by the moving windows, the data

330   are presented as the distribution function (fraction) then converted to percent for that window

331   length such that the binned ΔSST_{max} data sum to 100% over each window length. A 7-day

332   window was most likely to have a ΔSST_{max} of 2°C or less (82%), 14% of the data had a ΔSST_{max}

333   envelope of 3°C, and ~3% of the trajectories recorded a ΔSST_{max} of 4 °C. Over a 21-day window,

334   most trajectories had a ΔSST_{max} of 2-3ºC (combined account for 86% of data) and ~10% of the
335   trajectories had a ΔSST_{max} of 4-5ºC. As the window length increased, trajectories were more
336   likely to frequently have larger ΔSST_{max}. For the 45-day window lengths, ΔSST_{max} of 2-4ºC
337   were most common (83% of data), and for 90-day window lengths, ΔSST_{max} of 3-5ºC were most
338   common (61% of data). ΔSST_{max} reached as high as 9ºC for the 90-day windows but accounted
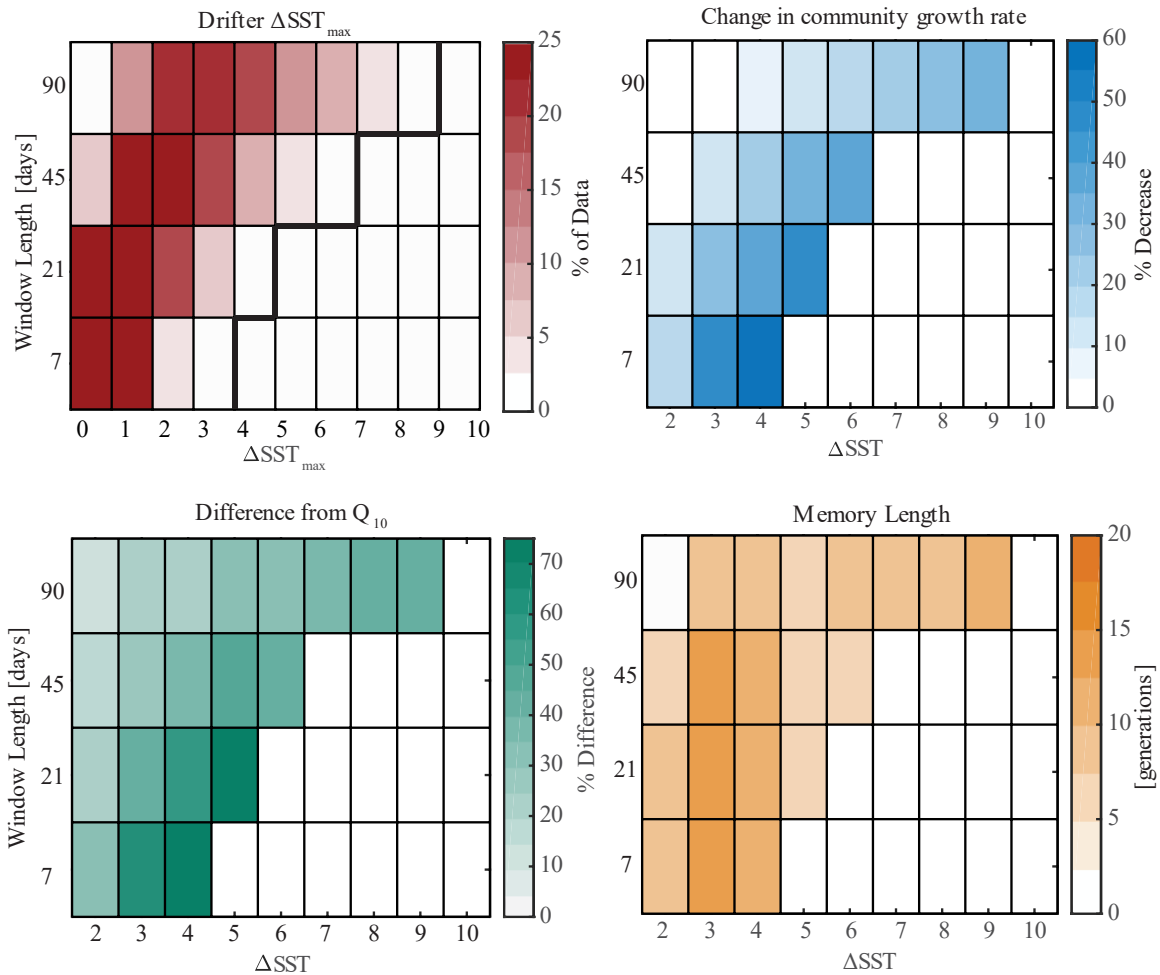339   for only 2.5% of the data in that window.

340

341

342   Figure 3. SST variability and the impact on growth rate and memory length for a skewed reaction norm
343   under increasing ΔSST conditions (see Supplemental Material for decreasing ΔSST and broad reaction
344   norm results). Panel (a) shows the frequency of ΔSST_{max} changes in the drifter data for different sized
345   windows. Data are presented as total percentage of data that fall within each window length bin such that
346   each row sums to 100%. Data to right of the thick black line are below a 2.5% occurrence rate and are
347   excluded from the other analyses. Panel (b) plots the decline in community growth rate in the phenotype
348   model that results from the SST moving out of the thermal niche of the original population (see Methods
349   and Figure S12). Data that are greyed out represent ΔSST and window length combinations that were not
350   supported by the results from panel (a). Panel (c) shows the percent difference between the Q_{10}
351   parameterized growth rate and the phenotype modeled community growth rates at the point where SST

352 stabilizes (see Figure S12 for example). Panel (d) plots the memory effect length associated with SST
353 changes in the idealized simulations. This represents the time it takes for the community growth rate to be
354 within 5% of the steady state growth rate at the final SST from the first time-step that SST is constant
355 (See Figure S12 for example).

356

357 Results from the ΔSST_{max} analysis for the satellite data showed that while the Lagrangian and
358 Eulerian reference frames largely recorded similar SST changes, the Lagrangian reference frame
359 was more likely to capture large ΔSST_{max} (Figure S10). For example, over a 7-day window,
360 ΔSST_{max} in a bin around 3°C was almost twice as likely to occur in the Lagrangian (14%) than in
361 the Eulerian (8%) reference frame. For the 21-day window, a ΔSST_{max} of 3-4°C was more likely
362 to occur in the Lagrangian (35%) reference frame than in the Eulerian (23%). Similarly, for the
363 45-day window, ΔSST_{max} of 2-4 ^{o}C were common in both, and larger changes of 4-5°C were
364 more common in the surface drifters (28%) than the satellite data (19%). Across the full 90 days,
365 ΔSST_{max} of 3-5 ^{o}C dominated the variability for both reference frames but the surface drifters
366 were twice as likely to record ΔSST_{max} beyond this range (29% of data) compared to the satellite
367 data (15%). Overall, while patterns of variability were similar, the Lagrangian reference frame
368 was more likely to record larger SST changes than the Eulerian. The larger SST changes
369 recorded in the Lagrangian reference frame impact phytoplankton community growth rates in a
370 different manner than the smaller SST changes that overlap between the two reference frames
371 (see Sections 3.2 and 3.3 below). Simulating phytoplankton growth with environmental
372 variability recorded in the Eulerian reference frame, as is common among many global
373 biogeochemical models, omits biologically relevant variability.

374

375 For most of the SST data recorded by the drifters, the rate of SST change was slower than the
376 expected phytoplankton acclimation rates. Acclimation rates for the Southern Ocean diatom *F.*
377 *cylindrus* range from 0.3^{o}C/day to 0.6^{o}C/day (Robert Strzepek, personal communication). For the
378 drifter trajectories, only 8% of all the days analyzed (n = 197,100 days) recorded daily rates of
379 SST change higher than 0.3^{o}C/day and less than 2% recorded daily rates of change larger than
380 0.6^{o}C/day (Figure S11). Because SST rates of change were typically slower than the
381 phytoplankton acclimation rate, we hypothesized that the rate of acclimation would not play a
382 major role in the community response. To simplify model dynamics, we ran our model with
383 rapid acclimation such that each phenotype responded directly to SST changes. See Section 4.1
384 for discussion about situations in which acclimation may be important.

385

386 *3.2 Idealized Simulations*

387 We used idealized simulations to develop a mechanistic understanding of how variability
388 impacts community growth rates. First, we used the idealized SST profiles to assess the impact
389 of changing SSTs on community growth rates by calculating the biomass-weighted community
390 growth rate (Eq. 5) at each timestep of the simulation. We found that SST rates of change larger

391   than 2-3°C in 45-90 days (or 28-57 generations at the stabilized growth rate of 0.5 day^{-1}), which
392   corresponded to a rate of SST change of 0.02-0.07 $^{\circ}$C/day, caused community growth rates to
393   decrease, regardless if SSTs were increasing or decreasing. Once SSTs stabilized at the final
394   value, community growth rates increased and eventually stabilized. We tracked the time required
395   for the community growth rate to reach ±5% of the stable value from the timestep at which SSTs
396   stabilized. This time lag or as we call it here, "memory effect", was then converted to
397   generations rather than days as this allowed us to understand the relative impact of temperature
398   change on phytoplankton using a common currency such that our results are not growth rate
399   dependent. We then compared the biomass-weighted community growth rates from the
400   phenotype model to the community growth rates calculated using the Q_{10} equation to test the
401   impact of rapid phenotype shifts on phytoplankton growth rates. We report only results for those
402   magnitudes of temperature change and durations of change that we observed in the drifter data
403   set (Figure 3a), specifically: ΔSST = 2-4°C in 7 days (0.29-0.57 $^{\circ}$C/day) , ΔSST = 2-5°C in 21
404   days (0.10-0.24 $^{\circ}$C/day) , ΔSST = 2-6°C in 45 days (0.04-0.13 $^{\circ}$C/day), and ΔSST = 2-9°C in 90
405   days (0.02-0.1 $^{\circ}$C/day). Uncertainty estimates reported here are the result of stochastic variability
406   from 100 simulations with different initial conditions. The results from the full range of ΔSSTs
407   are shown in the Supplemental Information (Figures S13 and S14).

408

409   *3.2.1 Impact of variable SSTs on community growth rates in the phenotype model*

410   For small, gradual SST changes of 2-3°C in 45-90 days (0.02-0.07 $^{\circ}$C/day), the community
411   growth rates changed linearly with the SST changes during the period of SST transition and then
412   stabilized once SST stopped changing. That is, the distribution of phenotypes within the
413   community changed at the same rate as the SST such that the T_{opt} of the most dominate
414   phenotype closely matched the SST. As a result, the temporal response in the community growth
415   rate from the phenotype model was similar to the growth rate from a null model using a
416   community Q_{10} parameterization which assumes rapid phenotype shifts in the community in
417   response to changing SST conditions. In all other simulations, when SST changed by more than
418   3°C, independent of the time over which this change occurred, a different pattern was observed.
419   Growth rates initially increased or decreased depending on the sign of the SST change, but then
420   began to decrease rapidly (see Figure S12 for example). The growth rates continued to decrease
421   until a minimum value was reached. This corresponded to when SSTs stabilized, after which
422   community growth rates increased to their final value and remained there for the rest of the
423   simulation. Growth rates decreased as much as 70% ±1% (1σ) during this low growth period
424   (Figure 3b) and a SST increase of 4°C in 7 days (0.57°C/day) resulted in the largest change
425   (Figure S13). While the absolute percent change in growth rate was partly due to our model
426   formulation, the qualitative results were robust and seen in the other ecosystem models we tested
427   (Figure S7).

428

429   Shifts in community growth rates were determined both by changes in the growth rates of
430   individual phenotypes (i.e. shifts along a reaction norm) and shifts in the community

431   composition (i.e. abundance of different phenotypes). The decrease in community growth rates
432   that accompanied both increases and decreases in SSTs was caused by the SSTs extending
433   beyond the thermal optimum of the initial community such that the bulk of the biomass was
434   growing slowly. During this period, the individual phenotypes with elevated growth rates only
435   made up a small fraction of the community and so did not contribute significantly to the
436   community growth rate. The community growth rates then rebounded as these high growth
437   phenotypes increased their biomass and eventually became the dominate biomass group. Faster
438   rates of SST change moved the community out of the thermal optimum of the initial community
439   more quickly than smaller rates of change, and therefore larger and faster ΔSSTs resulted in
440   greater decreases in community growth rates. However, the high growth individuals were able to
441   dominate the community more quickly due to the high loss rates for the slow (or no) growth
442   individuals and so the community growth rates rebounded more quickly than in the cases of
443   moderate SST change. For rapid SST changes, the rate and type of acclimation response could
444   potentially play a role in the shifts in community growth rates depending on the nature of the
445   plastic response (see *Discussion*).

446

447   *3.2.2 Memory Effect*

448   The overall magnitude and direction (increasing or decreasing) of SST change, combined with
449   time under transient conditions, and shape of the reaction norm (broad vs skewed) all played a
450   critical role in determining the length of the memory effect – defined here as the amount of time
451   for the community growth rate to stabilize. Critically, our results indicated that the most common
452   ΔSST changes (Figure 3a) were associated with the longest memory effects (Figure 3d). Nearly
453   all ΔSST values tested were sufficient to create a memory effect of longer than 2 generations,
454   and moderate changes of 3-4°C over 7-45 days or 4-28 generations (0.07-0.57 $^{\circ}$C/day) resulted in
455   the longest memory effects with slight differences between the reaction norm shapes (Figure 3d,
456   Figure S12). These moderate changes incurred the longest memory effect (up to 22 generations)
457   for both reaction norm shapes (decreasing SST, Figure S14) or up to nearly five times longer
458   than the duration of the ΔSST transient. Larger SST changes (5-6 $^{\circ}$C) that occurred over 45 or 90
459   days or 28-57 generations (0.06-0.13 $^{\circ}$C/day) tended to have slightly shorter memory effects (~8-
460   19 generations) than the moderate changes (3-4 $^{\circ}$C; 0.03-0.09 $^{\circ}$C/day) that occurred over the
461   same time frame (~10-23 generations). This difference was not statistically significant. Longer
462   memory effects for moderate SST changes resulted from dominant phenotypes in the previously
463   acclimated community being able to grow in the new environment, albeit at a reduced rate. This
464   made it harder for the phenotypes optimally suited for the new environment to become more
465   abundant, which resulted in larger memory effects. Communities that underwent large and rapid
466   temperature changes showed the largest short-term decline in community growth rates (Figure
467   S13) but also rebounded more quickly (i.e. had a shorter memory effect) than communities
468   experiencing moderate changes in SST (Figure S14).

469

470   The sign of the SST change also impacted the response time of the community. Decreasing
471   ΔSSTs had longer memory effects by an average of 7 generations compared to increasing ΔSSTs
472   (t-test, 95% CI) for the skewed shaped reaction norms. The longer memory effect was due to the
473   long tail on the decreasing side of the reaction norm, which allowed the phenotypes in the initial
474   community to grow during decreasing SST conditions (Figure S14). For reaction norms that
475   were symmetrical about the optimum growth temperature, the direction of ΔSST did not matter,
476   and the memory lengths were statistically the same for increasing and decreasing ΔSSTs (t-test,
477   95% CI) (Figure S14).

478

479   *3.2.3 Impact of assuming rapid phenotype shifts via Q_{10} model*

480   Using the Q_{10} equation (only a function of SST) to calculate community growth rates resulted in
481   perfect environmental tracking, or effectively (unrealistic) rapid phenotype shifts such that the
482   T_{opt} of the community perfectly followed SST (Figure S12). However, as discussed in Section
483   3.2.1, the timescales required for rearrangement of the community composition resulted in
484   decreased community growth rates in response to SST variability. To compare the Q_{10}
485   community growth rates to the phenotype-based model growth rates, we calculated the percent
486   difference between phenotype-based model and the Q_{10} model relative to the Q_{10} model (as $[(Q_{10}$
487   – phenotype)*100]/Q_{10}) at the time step when SSTs stabilize, which typically corresponds to the
488   time of minimum growth in the phenotype-based model (Figure 3c and S12). Community growth
489   rates derived from the Q_{10} model were always larger than those simulated by the phenotype
490   model, which was consistent with previous work that suggested that SST variability will result in
491   lower growth rates than when temperature variability is not considered (Moisan et al. 2002;
492   Bernhardt et al. 2018). However, the difference from Q_{10} was not constant but rather a function
493   of SST variability. As the ΔSST increased over a given window length, so did the difference
494   between the phenotype model and the Q_{10} model. The largest departures from Q_{10} occurred for
495   ΔSSTs of 4°C and 5 °C over 7 and 21 days, respectively, with up to 80% lower simulated
496   community growth rates for the phenotype model. The magnitude of this difference was
497   consistent with the modeling study of Moisan et al. (2002) who found that the Q_{10} growth rate
498   model over-estimated individual phenotype growth rates and population growth rates. The
499   smallest difference between the models was for ΔSST = 2 °C over 90 days which resulted in 2.5-
500   5% lower growth rates. Generally, larger ΔSSTs and faster rates of change (changes occurring
501   over a few generations) resulted in larger differences between the models.

502

503   *3.3 Southern Ocean Drifter Trajectories*

504   The idealized simulations allowed for a mechanistic explanation of the impact SST changes have
505   on phytoplankton community growth rates. However, in the ocean, SST change is much more
506   complicated as phytoplankton are exposed to a large variety of rates and duration of SST
507   changes. We used Southern Ocean drifter trajectories to investigate the impact of *in situ* SST
508   variability on community growth rates.

509   Using the Southern Ocean drifter trajectories, we found that, like the idealized simulations, the
510   phenotype model resulted in lower average community growth rates compared to the Q_{10} model
511   over the entire 90-days (Figure 4). Like the idealized simulations, as drifter SST variability
512   increased, so did the difference between the phenotype model and the Q_{10} model. The mean
513   percent difference between the phenotype model and the Q_{10} model for the trajectories ranged
514   between 9.0% - 39.8% for the skewed reaction norms. A similar pattern was observed for the
515   broad shaped reaction norms, but the magnitude of the difference was smaller and ranged from
516   just 0.6% to 24.6% different (Figure S15). Trajectories with higher mean SSTs were affected less
517   by SST variability than trajectories with lower SSTs. This was due to faster growth rates at
518   higher temperatures, which allowed more rapid responses to SST changes and shorter memory
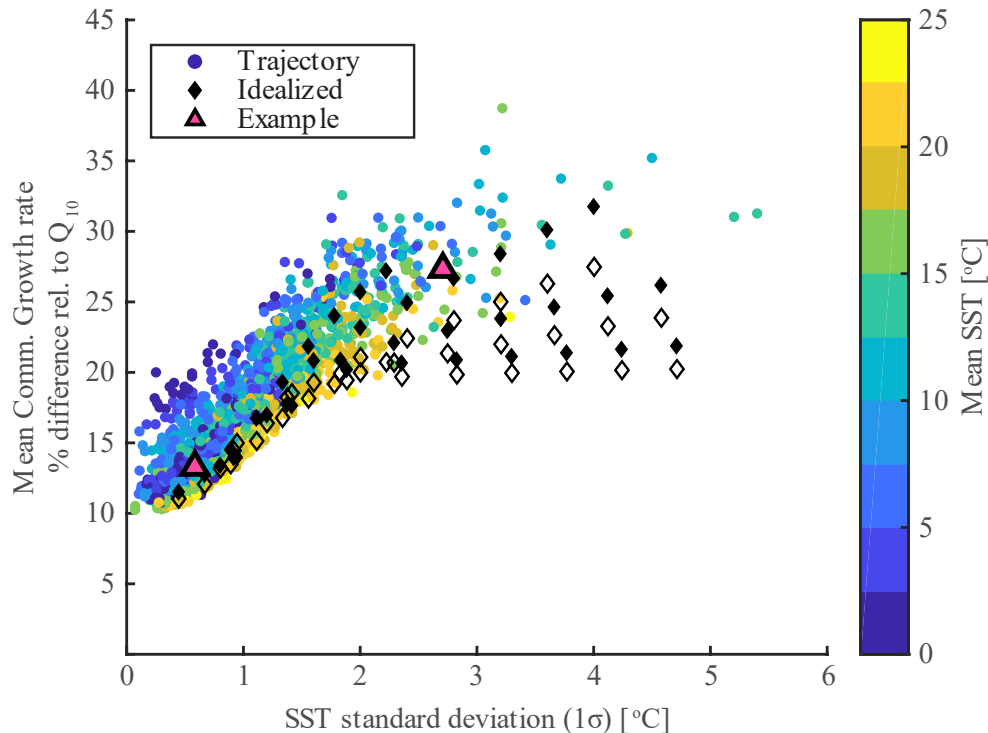519   lengths in terms of days (when normalized to generations there was no difference).

520

521

522   Figure 4. Impact of SST variability on community growth rate. The average percent difference in
523   community growth rate between the phenotype model and the Q_{10} growth model from the 90-day drifter
524   segments are plotted against the standard deviation (1σ) of the drifter SST. Each segment is colored by
525   the mean SST. Results from the idealized trajectories are shown as black circles with filled circles
526   denoting increasing SST trajectories and open circles denoting decreasing SSTs. Pink triangles represent
527   the two example trajectories from Figure 2. Results shown here are for skewed shaped reaction norms, see
528   Figure S15 for results for the broad shaped reaction norms.

529   To isolate the impact that short-term variability may have had on community growth rates
530   relative to longer-term shifts, we compared the 90-day mean biomass-weighted community

531 growth rate of the drifter trajectories to the smoothed splines derived from the trajectories. The
532 smoothed splines (i.e. low frequency variability) accounted for a varying percentage of the
533 overall SST variability from a median value of 27% when looking at a 1-day window to 93%
534 when looking at a 90-day window (Figure S16). We found that removing short-term variability
535 had no impact on community growth rates (t-test, 95% CI; Figure S17).

536

537 **4. Discussion**

538 *4.1 Impact of Acclimation*

539 Acclimation becomes potentially important when the rate of acclimation is slower than the rate
540 of SST change. To assess the potential impact of an acclimation timescale that was slower than
541 the SST change on our results, we ran the phenotype-based model with a range of acclimation
542 rates (0.2 $^{\circ}$C/day to 0.6 $^{\circ}$C/day (Robert Strzepek, personal communication) and ΔSST changes of
543 2-4°C in 7 days (0.29-0.57 $^{\circ}$C/day) and 5°C in 21 days (0.24 $^{\circ}$C/day) (Section S.7 in
544 Supplemental Material). The results were generally consistent with the rapid acclimation results
545 which suggested that acclimation timescales have a secondary impact on community growth
546 rates compared to phenotypic shifts. The slower acclimation rates did shift the balance between
547 phenotypic change in growth rate and the community composition shift (Section 3.2.1) and
548 resulted in both a delay in the decrease in community growth rates and a smaller magnitude
549 decrease (Figures 5a and S18). The memory effect increased linearly with a decrease in
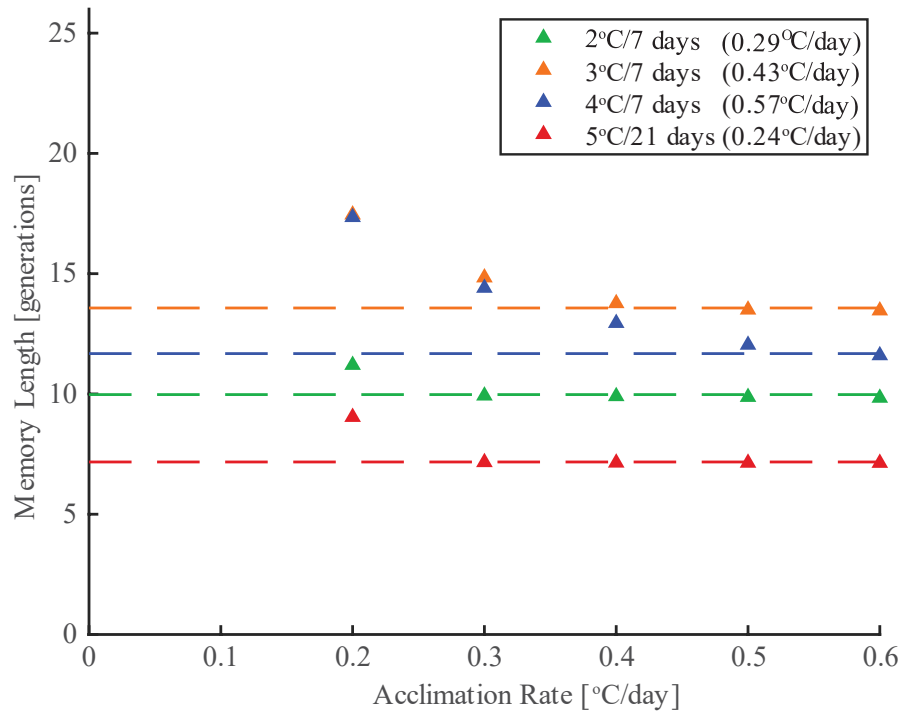550 acclimation rate (longer acclimation time) (Figures 5b and S19).

551

Figure 5. The impact of acclimation on memory lengths. Acclimation rates that were slower than the rate of SST change resulted in longer memory lengths than for simulations in which acclimation rate was equal to or faster than the SST rate of change.

The phenotypic plasticity represented in the model was a simplistic representation of plasticity. Specifically, we assumed that the phenotype slowly adjusted its growth rate by moving along the reaction norm at the rate defined by the acclimation timescale. As such, whether the plastic response was "beneficial" or "detrimental" (Kremer et al., 2018) depended on whether SSTs were increasing or decreasing and whether the initial SST was above or below T_{opt}. In reality, plastic responses are much more complex and nonlinear and most likely vary among species (Kremer et al., 2018). Additional work is needed to better constrain both the range or acclimation timescales and the mechanisms of phenotypic plasticity. However, our results suggest that these dynamics will only become important under rapid temperature changes which are infrequent in the ocean.

4.2 Implications for in-situ *community composition*

Our findings support the important role of thermal history in shaping the response of phytoplankton communities to changes in temperature. We have shown that SST variability can lower community growth rates for tens of generations following SST perturbation. This indicates that, for many regions of the ocean, the phytoplankton community will not be fully acclimated to

573   local conditions as a result of the mismatch between timescales of physical variability and
574   biological response. This mismatch in timescales will be a function of the rate and magnitude of
575   variability that phytoplankton in the water mass were previously exposed to and may be reflected
576   in physiological properties such as optimum growth temperature or overall community growth
577   rate.

578

579   Our results also provide an important extension on the classic principle that "everything is
580   everywhere: but the environment selects" (Hutchinson, 1961). Even when 'everything is
581   everywhere', we show that the timescale for environmental selection (community replacement)
582   is a critical factor in determining community composition. Specifically, we hypothesize that even
583   when the 'optimal' organism is present in an environment, SST variability generated by local
584   physics, lateral advection, and seasonal trends can delay or prevent that organism from
585   dominating the community. This hypothesis is supported by previous modeling work that has
586   shown a time-lag on the order of weeks to a month in the phytoplankton community growth
587   response to SST changes due to lateral advection and seasonal trends (Moisan, et al., 2002;
588   Hellweger et al. 2016). Here, we have quantified the relationship between varying rates of SST
589   variability and the timescale required for community replacement to impact the community
590   composition.

591

592   Underlying the time lag of the community response to SST variability were differences in the
593   distribution of phenotypes. When rates of change were slow, the community was able to keep up
594   with the changing SSTs and the T_{opt} of the most abundant phenotype matched the changing SSTs
595   (i.e. there is no memory effect and difference from Q_{10} is small). However, as SSTs became
596   more variable, the dynamics described above (Section 3.2) resulted in a mismatch between *in*
597   *situ* SST and the T_{opt} of the dominant phenotype (which resulted in larger offsets from Q_{10} and a
598   memory effect). Further, our results indicated that the difference in the nature of SST variability
599   between the Eulerian and Lagrangian reference frames could cause different community growth
600   rates and phenotype distribution.

601

602   The influence of lateral advection on the phenotype distribution of the community was evaluated
603   by comparing differences in the offset between the T_{opt} of the most abundant phenotype and the
604   SST of the simulation. We compared the SST at the end of each 90-day segment to the
605   phenotype T_{opt} offset (defined as SST minus T_{opt} of the most abundant phenotype at the final
606   time step). While the final SST of the drifter segments and satellite data were not statistically
607   different (t-test, 95% CI, Figure S20), differences in the nature of variability in the proceeding 90
608   days resulted in a significant difference between the final SST and the T_{opt} of the most abundant
609   phenotype (t-test, 95% CI, Figures 6 and S21). The magnitude of the offset between SST and T_{opt}
610   depended on the timing of SST changes throughout the 90-day profiles. Consistent with the
611   results from the idealized simulations, when SST changes were slow, the offset between SST and

612   the T_{opt} of the most abundant phenotype were negligible (Figure S22 for an example) while
613   larger and/or faster SST changes resulted in larger offsets (Figure S23 for an example). Large
614   SST changes that occurred early in the 90-day segment allowed sufficient time for the
615   community to respond and for the T_{opt} of the community to reflect the SST change, assuming the
616   SST profile stayed relatively stable after the initial SST change (see drifter data in Figure S22).
617   When SST changes occurred later in the 90-days, the community did not have sufficient time to
618   respond which caused a larger offset between the SST at day 90 and the T_{opt} of the community
619   (see satellite data in Figure S23). Different phenotype distributions for the Eulerian versus
620   Lagrangian reference frames is consistent with previous results that showed advection of
621   phytoplankton communities was a key process in shaping phytoplankton diversity (Barton et al.,
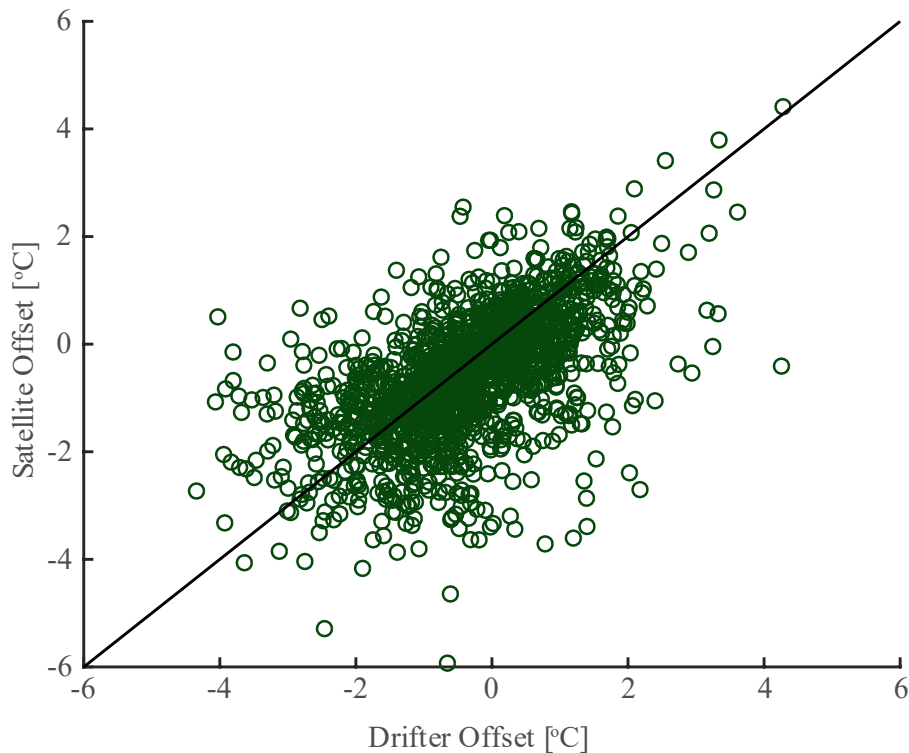622   2010; Clayton et al., 2013; Lévy et al., 2014).

623

625   Figure 6. The impact of Lagrangian and Eulerian variability on community composition. Here we plot the
626   difference between the Topt of the most abundant phenotype at the end of each 90-day trajectory and the
627   final SST for the drifter trajectory (x-axis) and the satellite data (y-axis). The final SSTs for the drifter and
628   satellite data are statistically identical (t-test, 95% CI). Therefore, deviations from the 1:1 line
629   demonstrate the impact of a Lagrangian versus Eulerian reference frame on community composition.

630

631   Our results support the hypothesis of Moisan et al. (2002) that the shape of the temperature
632   reaction norms has a significant impact on the community response to temperature variability.

633 Additionally, we suggest that the nature of the environmental variability may play an important
634 role in determining which reaction norm shapes will be most regionally competitive.
635 Specifically, under decreasing temperatures, a phenotype with a skewed reaction norm (T_{opt} is
636 closer to T_{max}) is predicted to have a competitive advantage over a phenotype with a broad
637 reaction norm (T_{opt} at the center of the range), given the same range and T_{opt}. The increased
638 competitive advantage is because the skewed reaction norm provides a larger range of
639 temperatures less than T_{opt} under which the phenotype can grow and, consequentially, a more
640 gradual decline in growth rate as a function of decreasing temperatures. Therefore, organisms
641 with skewed reaction norms should be adapted to have T_{opt} values close to maximum
642 encountered temperatures not only due to the rapid drop in growth rates for temperatures greater
643 than T_{opt} (Thomas et al., 2012) but also due to the competitive advantage under temperatures less
644 than T_{opt} (Moisan et al., 2002). Conversely, broad reaction norms are favored when temperatures
645 are warming, as expected, or when temperatures are more variable. Our results have
646 implications for the global distribution of reaction norm shapes. One would expect more skewed
647 reaction norms in the tropics where the warmest waters are found making it easier to evolve a
648 T_{opt} close to the maximum encountered temperature as this upper bound is constrained (Thomas
649 et al., 2012). However, in the polar regions where the temperatures encountered by
650 phytoplankton is much more variable, there should be selective pressure for broad reaction
651 norms with large growth ranges beyond T_{opt} as suggested by Moisan et al. (2002) or skewed
652 reaction norms where T_{opt} is higher than mean SSTs (Thomas et al., 2012).

653

654 *4.3 Implications for simulating community growth rates in global biogeochemical models*

655 The Q_{10} temperature-growth response is widely used in ecosystem models. The premise behind
656 employing a Q_{10} growth equation is that each modeled functional group encompasses many
657 species or strains with successive optimum growth temperatures. Therefore, a temperature
658 change will merely shift the distribution of species/strains in the group such that the one with a
659 T_{opt} matching the new temperature will dominate the community. However, as we have
660 demonstrated, the timescale of this shift is important and is a function of the rate, magnitude, and
661 direction of temperature change and the shape of the species/strains' thermal response curve. As
662 a result, this succession does not occur as rapidly as represented by the Q_{10} function. In fact,
663 community growth rates often temporarily declined until the phenotype with T_{opt} near ambient
664 conditions overcame the previously accumulated biomass. Because of the temporary decrease in
665 community growth rates, the Q_{10} temperature-growth response not only overestimates
666 temperature-related community growth but does so as a function of SST, SST variability, and
667 reaction norm shape. Critically, this indicates that adjusting the Q_{10} relationship to use a lower
668 exponent as previously suggested (Sherman et al., 2016) will only partially capture realistic
669 dynamics.

670

671 In addition to not capturing the full effect of SST variability on growth rates, biogeochemical
672 models may not be adequately capturing relevant variability. The current framework of most

673   biogeochemical models requires them to be integrated in an Eulerian reference frame. We have

674   shown that the Eulerian variability can differ substantially from the Lagrangian reference frame

675   (Figure S11). While the overall magnitude of the variability was similar between the Eulerian

676   and Lagrangian reference frames, we also found that the character of that variability was

677   different (Figure S11) and the Lagrangian reference frame recorded more variability that

678   generated longer memory effects in the phytoplankton community growth rates. The spatial

679   patterns of SST variability in the Southern Ocean were similar between Eulerian and Lagrangian

680   reference frames (Figure 7a,c) as was the effect on community growth rates (Figure 7b,d).

681   However, due to the dampened variability in the Eulerian reference frame relative to the

682   Lagrangian reference frame, the offset between community growth rates simulated using the Q_{10}

683   equation and the phenotype model was also lessened. Models such as DARWIN (Follows et al.,

684   2007) resolve phenotypes with a range of thermal reaction norms and so will capture the

685   community growth rate dynamics presented here. However, additional work is needed to

686   compare the variability encountered by functional group phenotypes in large-scale models

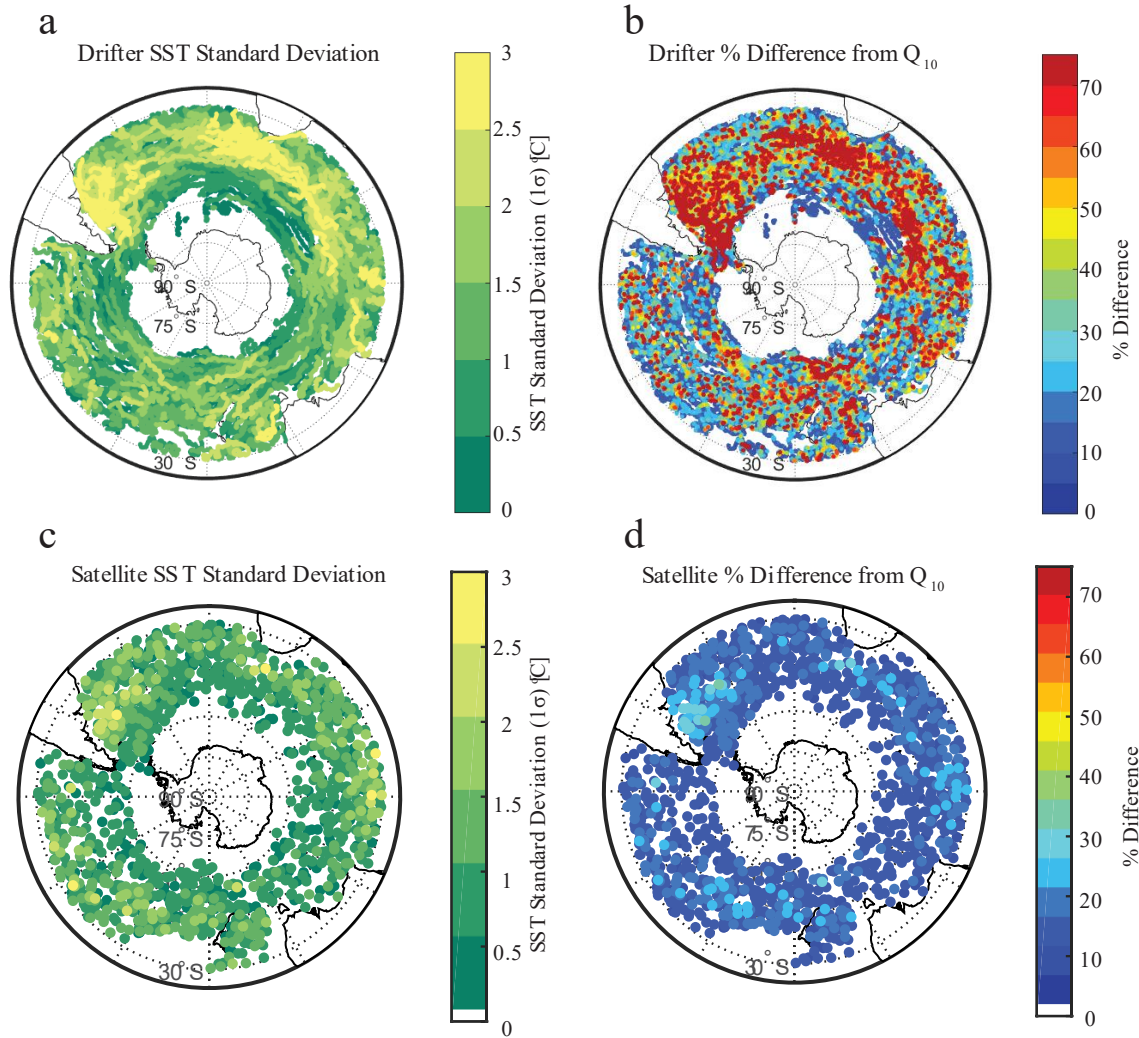687   integrated in an Eulerian framework to true Lagrangian variability.

688

Figure 7. Distribution of SST variability (a, c) and the deviation in community growth rate from Q_{10} (b, d) over the Southern Ocean (>30°S). Top row shows drifter data and bottom row shows satellite data. Three key regions of high SST variability stand out: Malvinas-Brazil confluence zone, the Agulhas Retroflection, and the Subtropical front. These regions have enhanced SST variability in both datasets but higher variability in the drifters. These high variability regions correspond to large differences between the phenotype model growth rates and Q_{10}.

Improving the parameterized temperature-growth relationship may be particularly important in the Southern Ocean. We used the model results described above to identify key regions within the Southern Ocean that might be most strongly impacted by temperature variability. Three particular regions stand out that exhibited the most SST variability and had the largest relative deviations from the Q_{10} model: the Malvinas-Brazil confluence zone; the Agulhas Retroflection region; and downstream from these two along the Subtropical Front near ~45°S, 60°E (Figures 7a,b). All three regions were previously identified as highly dynamic, strong frontal regions (Artana et al., 2019; Beal et al., 2015; Graham & Boer, 2013) and shown to be important hot-

705   spots for phytoplankton diversity (Barton et al., 2010; Clayton et al., 2013; d'Ovidio et al., 2010;
706   Soccodato et al., 2016). These regions represent the boundaries where cold, fresh polar water
707   meets the warm, salty subtropical where abundant mixing via meso- and sub-mesoscale
708   processes can occur (Clayton et al., 2017; d'Ovidio et al., 2010) and lead to the highly variable
709   SSTs recorded by the floats. It is possible that in these highly dynamic frontal regions the floats
710   were subjected to physical movements across the fronts that was previously thought to elude
711   phytoplankton movements. However, recent field and modeling studies have shown that cross-
712   front transfer and diapycnal mixing can occur due to the fine-scale physics associated with these
713   strong fronts (Clayton et al., 2017; Mahadevan, 2016; Wenegrat et al., 2020)

714

715   Our results also showed that large SST changes were not required for temperature variations to
716   have a lasting impact on community growth rates. While large differences between Q_{10}
717   community growth rates and the phenotype-based model community growth rates were common
718   in the regions mentioned above, other regions of the Southern Ocean that had moderate (2-3.5
719    $^{\circ}$C, 1σ) SST variability also recorded equally large differences in community growth rate, often
720   at least 45% smaller than Q_{10} estimates and up to 94.5% different. This was consistent with our
721   results from the idealized simulations which showed that moderate temperature changes can have
722   large impacts on community growth rates.

723

5. Conclusions

725   In this study we utilized idealized SST simulations and SST data from ocean surface drifters to
726   show that synoptic SST variability on time-scales of a few days to a few weeks temporarily
727   decreases phytoplankton community growth rates, while higher frequency variability has little
728   impact. The time it took for the community growth rate to reflect the new environment was
729   dependent upon the rate and magnitude of temperature change, the direction of change, and the
730   shape of the species/strains' thermal response curve. The largest memory effects resulted from
731   moderate changes in SST that occur over 1-3 weeks. This impact of SST variability can
732   potentially cause a large offset between a phenotype-based temperature-dependent community
733   growth rate and a Q_{10} based estimate and suggests that phytoplankton communities sampled *in*
734   *situ* may often not be adjusted to local conditions. Given the highly variable nature of the ocean
735   and importance of environmental variability for phytoplankton physiology, it is critical to
736   consider the correct reference frame and the magnitude and duration of variability when studying
737   phytoplankton dynamics. Here we demonstrated that the Lagrangian reference frame captured by
738   drifters was, in many instances, not equivalent to the Eulerian frame and that this had significant
739   impacts for estimating phytoplankton growth rates.

740

741

742

743 **Acknowledgements:**

754

755

756

757

758

759

760

761

762

763

764

765

766

767

768

769

770

771

772

773

774

775

776

777 Figure 1. The impact of SST variability on individual phenotype growth rate. (a) The
778 temperature related growth response for a phenotype with a skewed shaped reaction norm. The
779 values for the optimum growth temperature (T_{opt}) and the corresponding maximum growth rate
780 (μ_{max}) are shown with dashed lines. (b) The 90-day SST profile of an example drifter trajectory
781 (black) and the associated changes in phenotype growth rate (blue). The orange and red arrows in
782 the top panel indicate the change in the phenotype growth rate associated with the corresponding
783 changes in SST in the bottom panel.

784 Figure 2. a) Map of all 90-day drifter trajectories (n = 2190) colored by SST. Two example
785 trajectories are highlighted in purple and magenta. b) Reaction norms for each of the 319
786 phenotypes in the ecosystem model. The grey lines represent all the phenotype reaction norms
787 and the green lines are example phenotypes to highlight the reaction norm shape. c and d)
788 Example trajectories and their resulting model outputs. The top panels show the SST (colors), the
789 community growth rate simulated by Q_{10} method (dashed line), and the community growth rate
790 from our phenotype-based model (solid line). The bottom panel shows the growth rate through
791 time of each phenotype (grey lines). The blue line follows the phenotype with the highest initial
792 biomass, the red dashed line follows the phenotype that has the highest biomass at the end of the
793 90 days, and the green line follows the phenotype that has a T_{opt} equal to the mean SST of the
794 trajectory.

795 Figure 3. SST variability and the impact on growth rate and memory length for a skewed
796 reaction norm under increasing ΔSST conditions (see Supplemental Material for decreasing
797 ΔSST and broad reaction norm results). Panel (a) shows the frequency of ΔSSTmax changes in
798 the drifter data for different sized windows. Data are presented as total percentage of data that
799 fall within each window length bin such that each row sums to 100%. Data to right of the thick
800 black line are below a 2.5% occurrence rate and are excluded from the other analyses. Panel (b)
801 plots the decline in community growth rate in the phenotype model that results from the SST
802 moving out of the thermal niche of the original population (see Methods and Figure S12). Data
803 that are greyed out represent ΔSST and window length combinations that were not supported by
804 the results from panel (a). Panel (c) shows the percent difference between the Q10 parameterized
805 growth rate and the phenotype modeled community growth rates at the point where SST
806 stabilizes (see Figure S12 for example). Panel (d) plots the memory effect length associated with
807 SST changes in the idealized simulations. This represents the time it takes for the community
808 growth rate to be within 5% of the steady state growth rate at the final SST from the first time-
809 step that SST is constant (See Figure S12 for example).

810 Figure 4. Impact of SST variability on community growth rate. The average percent difference in
811 community growth rate between the phenotype model and the Q_{10} growth model from the 90-day
812 drifter segments are plotted against the standard deviation (1σ) of the drifter SST. Each segment
813 is colored by the mean SST. Results from the idealized trajectories are shown as black circles
814 with filled circles denoting increasing SST trajectories and open circles denoting decreasing
815 SSTs. Pink triangles represent the two example trajectories from Figure 2. Results shown here

816   are for skewed shaped reaction norms, see Figure S15 for results for the broad shaped reaction
817   norms.

818   Figure 5. The impact of acclimation on memory lengths. Acclimation rates that were slower than
819   the rate of SST change resulted in longer memory lengths than for simulations in which
820   acclimation rate was equal to or faster than the SST rate of change.

821   Figure 6. The impact of Lagrangian and Eulerian variability on community composition. Here
822   we plot the difference between the Topt of the most abundant phenotype at the end of each 90-
823   day trajectory and the final SST for the drifter trajectory (x-axis) and the satellite data (y-axis).
824   The final SSTs for the drifter and satellite data are statistically identical (t-test, 95% CI).
825   Therefore, deviations from the 1:1 line demonstrate the impact of a Lagrangian versus Eulerian
826   reference frame on community composition.

827   Figure 7. Distribution of SST variability (a, c) and the deviation in community growth rate from
828   Q_{10} (b, d) over the Southern Ocean (>30°S). Top row shows drifter data and bottom row shows
829   satellite data. Three key regions of high SST variability stand out: Malvinas-Brazil confluence
830   zone, the Agulhas Retroflection, and the Subtropical front. These regions have enhanced SST
831   variability in both datasets but higher variability in the drifters. These high variability regions
832   correspond to large differences between the phenotype model growth rates and Q_{10}.

833

834

835

836

837

838

839   Artana, C., Provost, C., Lellouche, J., Rio, M., Ferrari, R., & Sennéchael, N. (2019). The Malvinas

840   Current at the confluence with the Brazil Current: Inferences from 25 years of Mercator ocean

841   reanalysis. *Journal of Geophysical Research: Oceans*, *124*(10), 7178–7200.

842   https://doi.org/10.1029/2019JC015289

843   Barton, A. D., Dutkiewicz, S., Flierl, G., Bragg, J., & Follows, M. J. (2010). Patterns of diversity in

844   marine phytoplankton. *Science*, *327*(5972), 1509–1511. https://doi.org/10.1126/science.1184961

845   Beal, L. M., Elipot, S., Houk, A., & Leber, G. M. (2015). Capturing the transport variability of a western

846   boundary jet: Results from the Agulhas Current Time-Series experiment (ACT). *Journal of*

847   *Physical Oceanography*, *45*(5), 1302–1324. https://doi.org/10.1175/JPO-D-14-0119.1

848   Bernhardt, J. R., Sunday, J. M., Thompson, P. L., & O'Connor, M. I. (2018). Nonlinear averaging of

849   thermal experience predicts population growth rates in a thermally variable environment.

850   *Proceedings of the Royal Society B: Biological Sciences*, *285*(20181076), 10.

851   Boyd, P. W. (2019). Physiology and iron modulate diverse responses of diatoms to a warming Southern

852   Ocean. *Nature Climate Change*, *9*(2), 148–152. https://doi.org/10.1038/s41558-018-0389-1

853   Boyd, P. W., Cornwall, C. E., Davison, A., Doney, S. C., Fourquez, M., Hurd, C. L., Lima, I. D., &

854   McMinn, A. (2016). Biological responses to environmental heterogeneity under future ocean

855   conditions. *Global Change Biology*, *22*(8), 2633–2650. https://doi.org/10.1111/gcb.13287

856   Clayton, S., Dutkiewicz, S., Jahn, O., & Follows, M. J. (2013). Dispersal, eddies, and the diversity of

857   marine phytoplankton. *Limnology and Oceanography: Fluids and Environments*, *3*(1), 182–197.

858   https://doi.org/10.1215/21573689-2373515

859   Clayton, S., Lin, Y.-C., Follows, M. J., & Worden, A. Z. (2017). Co-existence of distinct Ostreococcus

860   ecotypes at an oceanic front. *Limnology and Oceanography*, *62*(1), 75–88.

861   https://doi.org/10.1002/lno.10373

862   d'Ovidio, F., De Monte, S., Alvain, S., Dandonneau, Y., & Levy, M. (2010). Fluid dynamical niches of

863   phytoplankton types. *Proceedings of the National Academy of Sciences*, *107*(43), 18366–18370.

864   https://doi.org/10.1073/pnas.1004620107

865   Deser, C., Alexander, M. A., Xie, S.-P., & Phillips, A. S. (2010). Sea surface temperature variability:

866   patterns and mechanisms. *Annual Review of Marine Science*, *2*(1), 115–143.

867   https://doi.org/10.1146/annurev-marine-120408-151453

868   Doblin, M. A., & van Sebille, E. (2016). Drift in ocean currents impacts intergenerational microbial

869   exposure to temperature. *Proceedings of the National Academy of Sciences*, *113*(20), 5700–5705.

870   https://doi.org/10.1073/pnas.1521093113

871   Eppley, R. (1972). Temperature and phytoplankton growth in the sea. *Fishery Bulliten*, *70*(4), 1063–1085.

872   Follows, M. J., Dutkiewicz, S., Grant, S., & Chisholm, S. W. (2007). Emergent biogeography of

873   microbial communities in a model ocean. *Science*, *315*(5820), 1843–1846.

874   https://doi.org/10.1126/science.1138544

875   Graham, R. M., & Boer, A. M. D. (2013). The dynamical subtropical front. *Journal of Geophysical*

876   *Research: Oceans*, *118*(10), 5676–5685. https://doi.org/10.1002/jgrc.20408

877   Hellweger, F. L., van Sebille, E., Calfee, B. C., Chandler, J. W., Zinser, E. R., Swan, B. K., & Fredrick,

878   N. D. (2016). The role of ocean currents in the temperature selection of plankton: Insights from

879   an individual-based model. *PLOS ONE*, *11*(12), e0167010.

880   https://doi.org/10.1371/journal.pone.0167010

881   Hutchinson, G. E. (1961). The paradox of the plankton. *The American Naturalist*, *95*(882), 137–145.

882   https://doi.org/10.1086/282171

883   Kling, J. D., Lee, M. D., Fu, F., Phan, M. D., Wang, X., Qu, P., & Hutchins, D. A. (2019). Transient

884   exposure to novel high temperatures reshapes coastal phytoplankton communities. *The ISME*

885   *Journal*. https://doi.org/10.1038/s41396-019-0525-6

886   Kremer, C. T., Fey, S. B., Arellano, A. A., & Vasseur, D. A. (2018). Gradual plasticity alters population

887   dynamics in variable environments: Thermal acclimation in the green alga *Chlamydomonas*

888   *reinhartdii. Proceedings of the Royal Society B: Biological Sciences*, *285*(1870), 20171942.

889   https://doi.org/10.1098/rspb.2017.1942

890   Kroeker, K. J., Bell, L. E., Donham, E. M., Hoshijima, U., Lummis, S., Toy, J. A., & Willis-Norton, E.

891   (2020). Ecological change in dynamic environments: Accounting for temporal environmental

892   variability in studies of ocean change biology. *Global Change Biology*, *26*(1), 54–67.

893   https://doi.org/10.1111/gcb.14868

894   Laufkötter, C., Vogt, M., Gruber, N., Aita-Noguchi, M., Aumont, O., Bopp, L., Buitenhuis, E., Doney, S.

895   C., Dunne, J., Hashioka, T., Hauck, J., Hirata, T., John, J., Le Quéré, C., Lima, I. D., Nakano, H.,

896   Seferian, R., Totterdell, I., Vichi, M., & Völker, C. (2015). Drivers and uncertainties of future

897   global marine primary production in marine ecosystem models. *Biogeosciences*, *12*(23), 6955–

898   6984. https://doi.org/10.5194/bg-12-6955-2015

899   Lévy, M., Jahn, O., Dutkiewicz, S., & Follows, M. J. (2014). Phytoplankton diversity and community

900   structure affected by oceanic dispersal and mesoscale turbulence. *Limnology and Oceanography:*

901   *Fluids and Environments*, *4*(1), 67–84. https://doi.org/10.1215/21573689-2768549

902   Mahadevan, A. (2016). The impact of submesoscale physics on primary productivity of plankton. *Annual*

903   *Review of Marine Science*, *8*(1), 161–184. https://doi.org/10.1146/annurev-marine-010814-

904   015912

905   Moisan, J. R., Moisan, T. A., & Abbott, M. R. (2002). Modelling the effect of temperature on the

906   maximum growth rates of phytoplankton populations. *Ecological Modelling*, *153*(3), 197–215.

907   https://doi.org/10.1016/S0304-3800(02)00008-X

908   Pittera, J., Humily, F., Thorel, M., Grulois, D., Garczarek, L., & Six, C. (2014). Connecting thermal

909   physiology and latitudinal niche partitioning in marine Synechococcus. *The ISME Journal*, *8*(6),

910   1221–1236. https://doi.org/10.1038/ismej.2013.228

911 Qu, P., Fu, F.-X., Kling, J. D., Huh, M., Wang, X., & Hutchins, D. A. (2019). Distinct responses of the

912 nitrogen-fixing marine cyanobacterium Trichodesmium to a thermally variable environment as a

913 function of phosphorus availability. *Frontiers in Microbiology*, *10*, 1282.

914 https://doi.org/10.3389/fmicb.2019.01282

915 Reynolds, R. W., & Smith, T. M. (1994). Improved global sea surface temperature analyses using

916 optimum interpolation. *Journal of Climate*, *7*(6), 929–948. https://doi.org/10.1175/1520-

917 0442(1994)007<0929:IGSSTA>2.0.CO;2

918 Rohr, T., Harrison, C., Long, M. C., Gaube, P., & Doney, S. C. (2020a). Eddy-modified iron, light, and

919 phytoplankton cell division rates in the simulated Southern Ocean. *Global Biogeochemical*

920 *Cycles*, *34*(6), e2019GB006380. https://doi.org/10.1029/2019GB006380

921 Rohr, T., Harrison, C., Long, M. C., Gaube, P., & Doney, S. C. (2020b). The simulated biological

922 response to Southern Ocean eddies via biological rate modification and physical transport. *Global*

923 *Biogeochemical Cycles*, *34*(6), e2019GB006385. https://doi.org/10.1029/2019GB006385

924 Schaum, C.-E., Buckling, A., Smirnoff, N., Studholme, D. J., & Yvon-Durocher, G. (2018).

925 Environmental fluctuations accelerate molecular evolution of thermal tolerance in a marine

926 diatom. *Nature Communications*, *9*(1), 1719. https://doi.org/10.1038/s41467-018-03906-5

927 Sherman, E., Moore, J. K., Primeau, F., & Tanouye, D. (2016). Temperature influence on phytoplankton

928 community growth rates. *Global Biogeochemical Cycles*, *30*(4), 550–559.

929 https://doi.org/10.1002/2015GB005272

930 Soccodato, A., d'Ovidio, F., Lévy, M., Jahn, O., Follows, M. J., & De Monte, S. (2016). Estimating

931 planktonic diversity through spatial dominance patterns in a model ocean. *Marine Genomics*, *29*,

932 9–17. https://doi.org/10.1016/j.margen.2016.04.015

933 Thomas, M. K., Kremer, C. T., Klausmeier, C. A., & Litchman, E. (2012). A global pattern of thermal

934 adaptation in marine phytoplankton. *Science*, *338*(6110), 1085–1088.

935 https://doi.org/10.1126/science.1224836

936   Wang, X., Fu, F., Qu, P., Kling, J. D., Jiang, H., Gao, Y., & Hutchins, D. A. (2019). How will the key

937   marine calcifier Emiliania huxley; respond to a warmer and more thermally variable ocean?

938   *Biogeosciences*, *16*(22), 4393–4409. https://doi.org/10.5194/bg-16-4393-2019

939   Wenegrat, J. O., Thomas, L. N., Sundermeyer, M. A., Taylor, J. R., D'Asaro, E. A., Klymak, J. M.,

940   Shearman, R. K., & Lee, C. M. (2020). Enhanced mixing across the gyre boundary at the Gulf

941   Stream front. *Proceedings of the National Academy of Sciences*.

942   https://doi.org/10.1073/pnas.2005558117

943